The effect of high-frequency torsion in vibratory pile installation
The Gentle Driving of Piles method

Tsetas, Athanasios; Tsouvalas, Apostolos; Metrikine, Andrei

DOI
10.1088/1742-6596/2647/8/082012

Publication date
2024

Document Version
Final published version

Published in
Journal of Physics: Conference Series

The effect of high-frequency torsion in vibratory pile installation: the Gentle Driving of Piles method

Journal of Physics: Conference Series **2647** (2024) 082012 doi:10.1088/1742-6596/2647/8/082012

The effect of high-frequency torsion in vibratory pile installation: the Gentle Driving of Piles method

Athanasios Tsetas[1], **Apostolos Tsouvalas**[1], **Andrei Metrikine**[1]

[1]Faculty of Civil Engineering and Geosciences, Delft University of Technology, Stevinweg 1, Delft, 2628 CN, The Netherlands

E-mail: a.tsetas@tudelft.nl

Abstract. The Gentle Driving of Piles (GDP) is a new technology for vibratory (mono)pile installation that is based on simultaneous application of low-frequency/axial and high-frequency/torsional vibrations. In this paper, a numerical modelling framework, that has been developed and successfully applied to axial vibratory driving, is employed to study GDP. In that manner, the major driving mechanism of this method is comprehended on the basis of field observations and numerical analyses. As regards the numerical model, the pile is described as a thin cylindrical shell and the soil medium is treated as a linear elastic layered half-space. The pile-soil coupling is realized via a history-dependent frictional interface, that accounts for friction force degradation due to the accumulation of loading cycles at the soil material points. The redirection of the friction force vector due to the high-frequency torsion manifests as the main driving mechanism of GDP. Finally, the soil disturbance during installation is compared for the cases of GDP and axial vibratory driving, showcasing the dissimilar characteristics of the induced soil motion.

1. Introduction

Presently, over 80% of the offshore wind turbines in Europe are founded on monopiles [1]. These large tubular substructures are customarily installed via impact hammering [2]. In this piling method, a hammer is mounted on the pile top and the applied pulses progressively drive the pile into the seabed. Notwithstanding its simplicity and robustness, impact piling poses alarming problems related to pile structural damage and significant underwater noise emissions, which are harmful to aquatic species [3]. With a view to improve monopile installation in terms of performance and environmental aspects, alternative techniques are investigated. Vibratory pile driving is used onshore for decades and possesses advantageous features such as high installation speed and low axial pile stresses [4]. In offshore monopiles, vibratory installation is hindered by the incompleteness of available field observations and knowledge gaps related to drivability, energy efficiency and lateral pile response. To further boost the performance of vibratory methods, the Gentle Driving of Piles (GDP) has been proposed and tested successfully by TU Delft [5]. The GDP method is based on simultaneous application of low-frequency axial and high-frequency torsional vibrations, with a view to enhance installation performance and to reduce underwater noise emissions.

In this paper, the focus lies in the study of the GDP method with the aid of field data and numerical modelling. Medium-scale field tests have been executed at Maasvlakte II in the Port of Rotterdam, in which the proof of concept of the method was achieved [6]. In these experiments,

test piles were installed by means of GDP and conventional installation techniques, in order to facilitate their comparison. As regards the numerical modelling aspect, a 3-D axisymmetric model is presented for the drivability analysis of vibratory and GDP methods. In particular, the model is comprised by a thin cylindrical shell (pile), a linear elastic layered half-space (soil) and a history-dependent frictional interface. The coupled non-linear pile-soil problem is solved by a hybrid frequency-time approach based on sequential application of the Harmonic Balance Method (HBM). Comparison of numerical results against field data showcases the predictive potential of the approach and the model at hand is utilized to comprehend the mechanics of GDP. By virtue of the high-frequency torsional excitation, the friction force is diverted from the penetration axis, leading to the superb installation performance of GDP. Conclusively, a comparison between axial vibratory driving and GDP is presented in terms of induced ground motion to assess the environmental disturbance associated with the two techniques.

Figure 1: Pile installation at the GDP test site.

2. A numerical model for pile installation via axial vibro-driving and GDP

The Gentle Driving of Piles is a new vibratory pile installation technology that is founded on the simultaneous application of low-frequency/axial and high-frequency/torsional vibrations, with a view to improve the process of offshore monopile installation [5]. It is envisaged that torsion will reduce the soil reaction along the penetration axis, leading to enhanced installation performance and reduced noise emissions. An experimental campaign was designed and executed at Maasvlakte II in the Port of Rotterdam (see Fig. 1), with major highlights the remarkable installation and post-installation performances of the GDP piles in comparison with standard pile driving techniques [6, 7]. A detailed description of the first GDP shaker design (see Fig. 2) and the experimental findings of the GDP campaign can be found in [6].

In the ensuing, a numerical model is presented for GDP, that utilizes as a basis a newly developed approach for axial vibratory driving [8]. Consider a tubular pile with wall thickness h_p, length L_p and mid-surface radius R_p. The pile is described as a thin cylindrical shell based on the Love-Timoshenko theory [9], and is comprised by linear isotropic elastic material with Young's modulus E_p, Poisson's ratio ν_p and mass density ρ_p. The Semi-analytical Finite Element (SAFE) method is utilized to model the pile and the respective equations of motion read [8]:

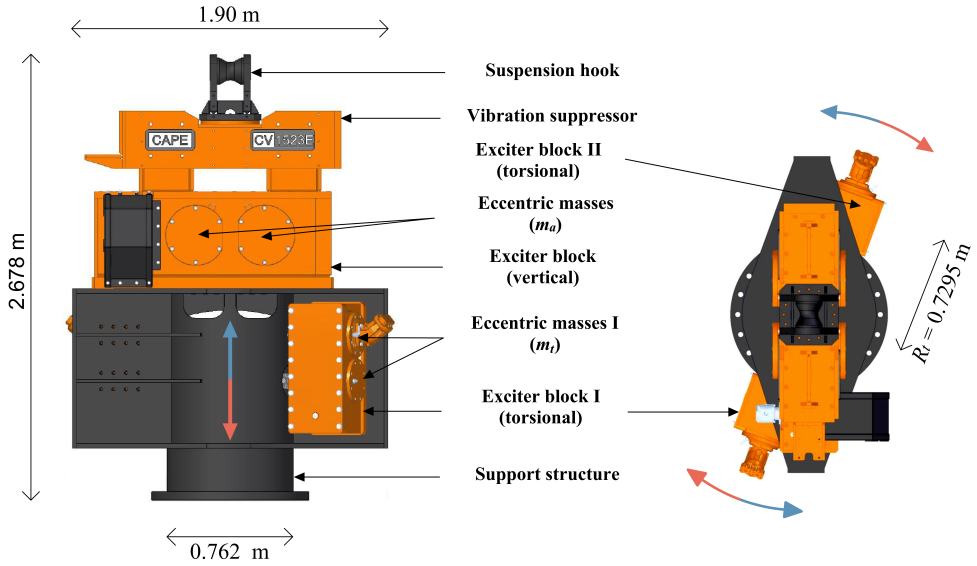

Figure 2: Detailed design of the GDP shaker.

$$\mathbf{I}^{\mathrm{s}}_{\mathrm{p},0}\frac{\mathrm{d}^2\mathbf{u}^{\mathrm{s}}_{\mathrm{p},0}}{\mathrm{d}t^2}+\mathbf{L}^{\mathrm{s}}_{\mathrm{p},0}\mathbf{u}^{\mathrm{s}}_{\mathrm{p},0}=\mathbf{p}^{\mathrm{s}}_{\mathrm{p},0} \tag{1a}$$

$$\mathbf{I}^{\mathrm{a}}_{\mathrm{p},0}\frac{\mathrm{d}^2\mathbf{u}^{\mathrm{a}}_{\mathrm{p},0}}{\mathrm{d}t^2}+\mathbf{L}^{\mathrm{a}}_{\mathrm{p},0}\mathbf{u}^{\mathrm{a}}_{\mathrm{p},0}=\mathbf{p}^{\mathrm{a}}_{\mathrm{p},0} \tag{1b}$$

where $\mathbf{I}^{\mathrm{s}}_{\mathrm{p},0}$, $\mathbf{I}^{\mathrm{a}}_{\mathrm{p},0}$ are the shell mass matrices, $\mathbf{L}^{\mathrm{s}}_{\mathrm{p},0}$, $\mathbf{L}^{\mathrm{a}}_{\mathrm{p},0}$ are the shell stiffness matrices, $\mathbf{u}^{\mathrm{s}}_{\mathrm{p},0}$, $\mathbf{u}^{\mathrm{a}}_{\mathrm{p},0}$ are the displacement/rotation vectors and $\mathbf{p}^{\mathrm{s}}_{\mathrm{p},0}$, $\mathbf{p}^{\mathrm{a}}_{\mathrm{p},0}$ are the vectors of consistent line forces/moments. The problem at hand is axisymmetric and the superscripts s and a denote the symmetric and anti-symmetric shell configurations, respectively [8]. It is remarked that the line force/moment vector also accommodates the non-linear pile-soil interaction forces. Finally, the full pile displacement/rotation vector $\mathbf{u}_{\mathrm{p}}$ and the line force/moment vector $\mathbf{p}_{\mathrm{p}}$ may be expressed as follows:

$$\mathbf{u}_{\mathrm{p}}=\begin{bmatrix}\mathbf{u}^{\mathrm{s}}_{0}\\ \mathbf{v}^{\mathrm{a}}_{0}\\ \mathbf{w}^{\mathrm{s}}_{0}\\ \boldsymbol{\beta}^{\mathrm{s}}_{z,0}\end{bmatrix},\quad \mathbf{p}_{\mathrm{p}}=\frac{1}{2\pi R_{\mathrm{p}}}\begin{bmatrix}\mathbf{p}^{\mathrm{s}}_{z0,\mathrm{p}}\\ \mathbf{p}^{\mathrm{a}}_{\theta 0,\mathrm{p}}\\ \mathbf{p}^{\mathrm{s}}_{r0,\mathrm{p}}\\ \mathbf{m}^{\mathrm{s}}_{zz0,\mathrm{p}}\end{bmatrix} \tag{2}$$

The soil medium is considered as a linear elastic layered half-space that interacts with the pile through non-linear shaft and tip formulations. The Thin-Layer Method (TLM) is employed to model the layered soil medium and its coupling with Perfectly Matched Layers (PMLs) is utilized to approximate the underlying half-space [10, 11]. By means of the TLM+PMLs approach, the Green's functions for ring sources are computed in the frequency-space domain [12]. Accordingly, the vectors of soil displacements $\widetilde{\mathbf{u}}_{r,\mathrm{s}}$, $\widetilde{\mathbf{u}}_{\theta,\mathrm{s}}$ and $\widetilde{\mathbf{u}}_{z,\mathrm{s}}$ can be expressed as follows:

$$\widetilde{\mathbf{u}}_{\mathrm{s}}=\begin{bmatrix}\widetilde{\mathbf{u}}_{r,\mathrm{s}}\\ \widetilde{\mathbf{u}}_{\theta,\mathrm{s}}\\ \widetilde{\mathbf{u}}_{z,\mathrm{s}}\end{bmatrix}=\begin{bmatrix}\widetilde{\mathbf{F}}_{rr} & \mathbf{0} & \widetilde{\mathbf{F}}_{rz}\\ \mathbf{0} & \widetilde{\mathbf{F}}_{\theta\theta} & \mathbf{0}\\ \widetilde{\mathbf{F}}_{zr} & \mathbf{0} & \widetilde{\mathbf{F}}_{zz}\end{bmatrix}\begin{bmatrix}\widetilde{\mathbf{p}}_{r,\mathrm{s}}\\ \widetilde{\mathbf{p}}_{\theta,\mathrm{s}}\\ \widetilde{\mathbf{p}}_{z,\mathrm{s}}\end{bmatrix} \tag{3}$$

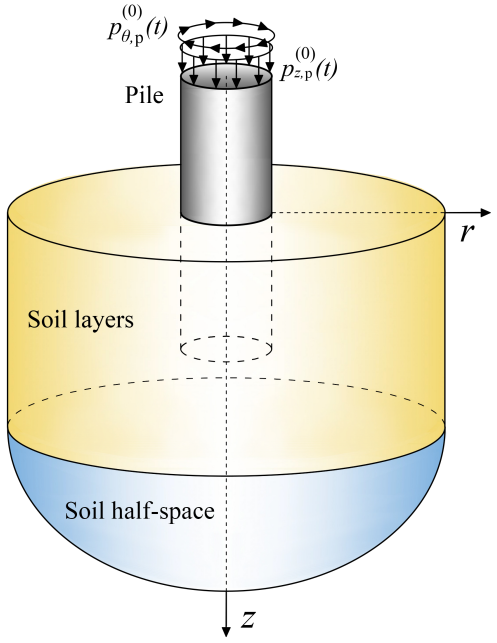

Figure 3: Installation of a pipe pile in a layered soil medium via vertical and torsional vibrations.

where $\widetilde{\mathbf{p}}_{r,\mathrm{s}}$, $\widetilde{\mathbf{p}}_{\theta,\mathrm{s}}$, $\widetilde{\mathbf{p}}_{z,\mathrm{s}}$ are the ring loads in the indicated directions and $\widetilde{\mathbf{F}}_{\mathrm{s}}$ denotes the dynamic flexibility matrix in the frequency-space domain. Due to the axisymmetric conditions, the uncoupling of axial-radial and circumferential motions leads to $\widetilde{\mathbf{F}}_{r\theta} = \widetilde{\mathbf{F}}_{\theta r} = \widetilde{\mathbf{F}}_{z\theta} = \widetilde{\mathbf{F}}_{\theta z} = \mathbf{0}$. Overall, the three motion components are coupled due to the non-linear pile-soil interaction forces, which are introduced in the force vector. The described model is depicted in Fig. 3.

As regards the pile-soil coupling, the following compatibility conditions are required to be satisfied during pile installation:
(i) continuity of radial displacements at the pile-soil interface:

$$\mathbf{w}^{\mathrm{c}} = \mathbf{u}^{\mathrm{c}}_{r}\Big|_{r=R_{\mathrm{p}}} \tag{4}$$

in which the superscript c denotes the part of pile and soil along the contact interface.

(ii) compatibility of vertical tractions applied at the pile-soil interface and at the pile tip:

$$\mathbf{p}^{\mathrm{c}}_{z,\mathrm{s}} = -\mathbf{p}^{\mathrm{c}}_{z,\mathrm{p}}, \quad p^{(\mathrm{t})}_{z,\mathrm{s}} = -p^{(\mathrm{t})}_{z,\mathrm{p}} \tag{5}$$

in which the superscript (t) denotes the tip related component.

(iii) compatibility of radial tractions applied at the pile-soil interface:

$$\mathbf{p}^{\mathrm{c}}_{r,\mathrm{s}} = -\mathbf{p}^{\mathrm{c}}_{r,\mathrm{p}} \tag{6}$$

(iv) compatibility of circumferential tractions applied at the pile-soil interface:

$$\mathbf{p}^{\mathrm{c}}_{\theta,\mathrm{s}} = -\mathbf{p}^{\mathrm{c}}_{\theta,\mathrm{p}} \tag{7}$$

The vertical tractions are dictated by a history-dependent frictional interface based on Coulomb friction, whereas the tip reaction follows an visco-elasto-plastic formulation [8]. Finally,

the numerical solution of the coupled problem is sought via the sequential application of the Alternating Frequency-Time (AFT) Harmonic Balance Method (HBM) [13]. For that purpose, we arrange all the residuals following from the pile-soil dynamic equilibria and the compatibility conditions in the residual vector $\mathbf{r}$ and require that its Fourier coefficients vanish, implying an approximate solution to our problem. These coefficients are obtained via a Fourier–Galerkin projection as follows:

$$\mathbf{R}_{\mathrm{F}} = \frac{1}{T_0} \int_0^{T_0} \mathbf{r}\mathbf{h} \, \mathrm{d}t \tag{8}$$

where $\mathbf{R}_{\mathrm{F}}$ is the Fourier coefficients matrix of the residuals, T_0 is the period corresponding to the base frequency of the HBM (Ω_0) and the row vector $\mathbf{h}$ encapsulates the test functions (i.e. Fourier harmonics) $h_j(t)$ defined as:

$$h_j(t) = \frac{1}{2}\left[\left(1+(-1)^j\right)\cos\left(\frac{j\Omega_0 t}{2}\right) + \left(1+(-1)^{j+1}\right)\sin\left(\frac{j+1}{2}\Omega_0 t\right)\right] \tag{9}$$

where j may correspond to any non-negative integer value up to the truncation limit. Further details regarding the numerical solution method can be found in [8] and will be omitted herein for the sake of brevity.

3. Numerical results and field data

In the ensuing, numerical results are compared with field data for the case of GDP. Furthermore, the main driving mechanism of GDP is showcased and a comparison study between the latter and axial vibro-driving is conducted, focusing on induced ground motion.

3.1. Pile drivability predictions for GDP

The field data collected during the GDP experimental campaign are considered in the following [6]. The pile properties can be found in Table 1, whereas the input excitation is inferred from strain measurements recorded during installation via fiber Bragg grating (FBG) sensors. During the site investigation, Seismic Cone Penetration Tests with pore water pressure measurements (SCPTu) were performed with a target depth of 10 m. Accordingly, the geotechnical properties of the installation locations can be seen in Fig. 4. As regards the material dissipation, both pile and soil possess frequency-independent hysteretic damping with ratios $\xi_{\mathrm{p}} = 0.001$ and $\xi_{\mathrm{s}} = 0.025$ (identical for P- and S-waves), respectively.

The presented modelling framework has been successfully applied to axial vibratory driving and benchmarked with field data [8]. By extending the model to introduce the circumferential motion of both pile and soil, the installation process of GDP can also be treated. Furthermore, the motivation to employ a common framework for these two approaches - i.e. axial vibro-driving and GDP - lies also in their inherent physical similarity. For that purpose, the (S)CPT-based soil reaction formulation for vibratory driving is also retained for the analysis of GDP. The comparison between the numerical results and the field data for two installation tests (GDP_1 and GDP_2) showcases that the present formulation can also be successfully applied for drivability predictions of GDP (see Fig. 5). The inflow of additional field data from future experiments will serve to further refine our approach and to build confidence for customary use in engineering practice.

3.2. The driving mechanism of GDP - friction force redirection

Following the favourable comparison between model output and field data, it is vital to comprehend the mechanism that leads to the promising installation performance of GDP.

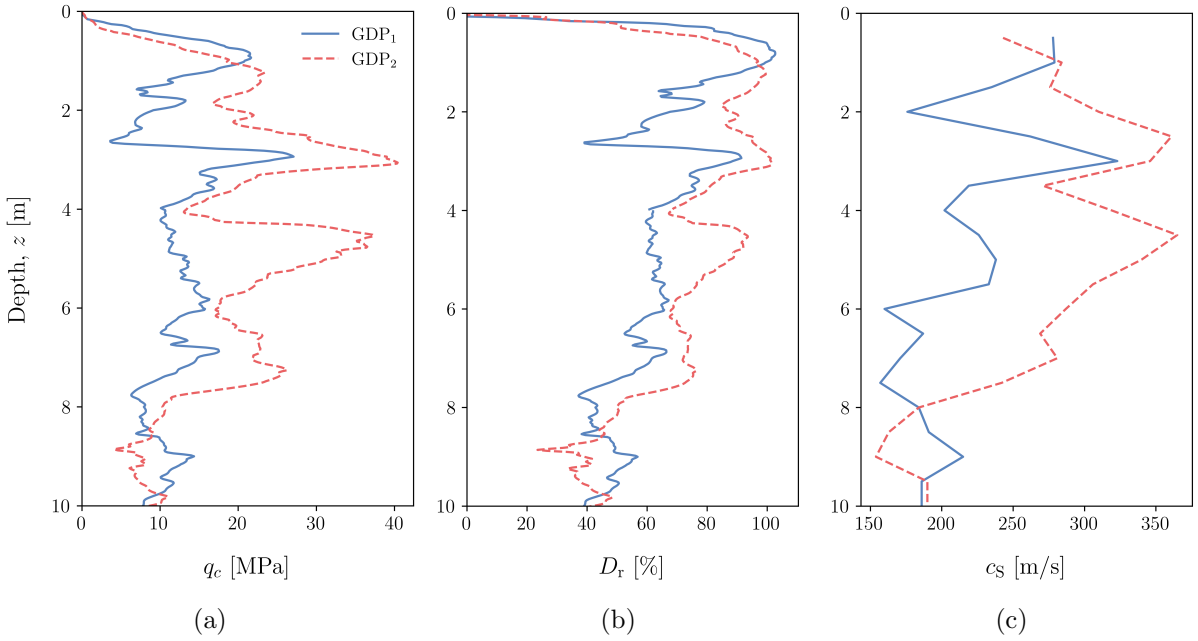

Figure 4: Profiles of (a) cone tip resistance (q_c), (b) relative density (D_r), and (c) shear wave velocity (c_S) obtained from the SCPTu's.

Table 1: Properties of the piles driven in the GDP field campaign.

ρ_p [kg/m^3]	E_p [Pa]	ν_p [-]	L_p [m]	R_p [m]	h_p [m]
7850	$210{\cdot}10^9$	0.3	10	0.373	0.0159

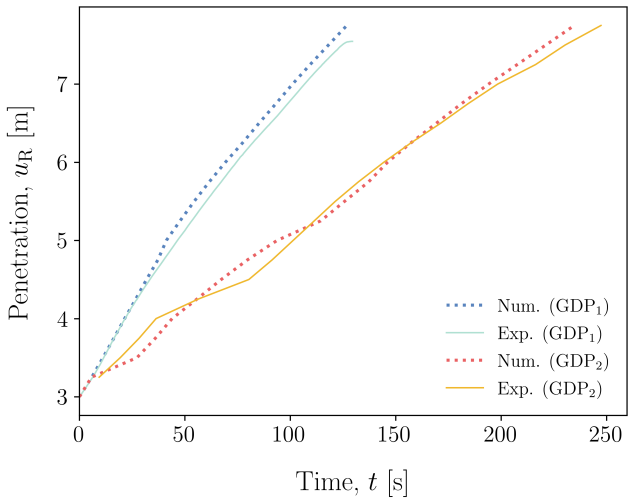

Figure 5: Comparison of numerical model predictions (Num.) with field data (Exp.) from the GDP experiments.

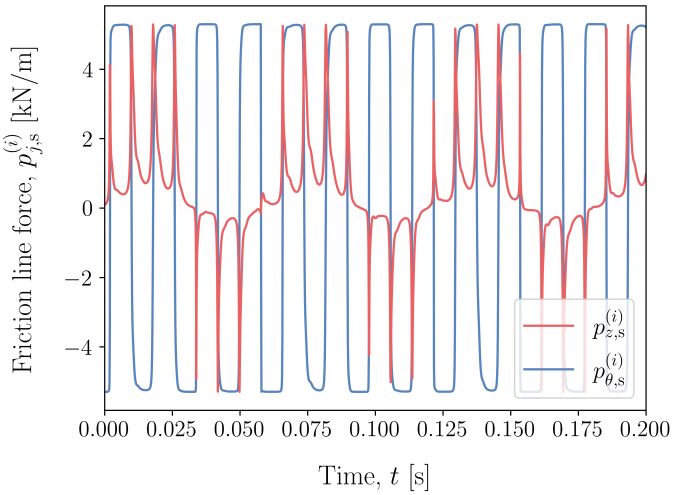

Figure 6: Friction force components ($p_{z,\mathrm{s}}^{(i)}$, $p_{\theta,\mathrm{s}}^{(i)}$) at $z_i = 3.0$ m and pile penetration $u_\mathrm{R} = 5.5$ m.

The torsional excitation implies frictional soil reaction along the circumferential direction, thus reduction of the vertical soil reaction is anticipated. On the premise of a hereditary Coulomb friction law, it is found that friction is predominantly mobilized in the circumferential direction and is accompanied by a significantly lower friction force along the vertical axis. In Fig. 6, both vertical and circumferential friction forces are shown at elevation of 3 m below the ground surface; the displayed time window corresponds to pile penetration of 5.5 m. These results are also visualized in terms of the the friction force trajectory in Fig. 7. As can be seen, the preponderance of the friction force data points cluster around two horizontal lines that correspond to zero vertical friction force and extrema of circumferential friction force. We conclude that the redirection of the friction force vector emerges as the major driving mechanism of GDP, as it leads to great reduction of the soil reaction along the penetration axis.

3.3. Comparison of ground motion between axial vibratory driving and GDP

The respective benchmarked models are employed to study the soil motion for vibro-driving and GDP. To eliminate the influence of dissimilar soil conditions, vibratory installation is realized numerically at the locations of piles GDP_1 and GDP_2; the respective vibro-driven piles are denoted as VH_1 and VH_2. The load amplitude is adjusted in vibro-driving to achieve a fairly similar penetration profile between VH and GDP piles. In the ensuing, we focus solely on the comparison between VH_1 and GDP_1 due to space limitations. As regards the driving frequencies, the torsional excitation for GDP_1 is applied at $f_\mathrm{t} = 62.6$ Hz, whereas the axial excitation frequencies are $f_\mathrm{a} = 24.8$ Hz and $f_\mathrm{a} = 16.3$ Hz for VH_1 and GDP_1, respectively. More details on the specifications of the vibratory and GDP devices can be found in [6].

In Fig. 8, the peak particle velocities (PPVs) are presented throughout the soil domain (i.e. surface and interior) as contours in the $r - z$ plane for both driving methods. As can be seen, the PPV amplitudes are largely reduced for GDP_1, with a notable abatement of the surface motion. The latter implies diminishing of the surface Rayleigh waves and results from the friction redirection in GDP. In particular, high-frequency SH waves are elicited by torsion, which lead to reduction of the overall SV-P wavefield and transfer of energy in higher frequencies. The preceding also serve to comprehend the more localized disturbance in the case of GDP, by virtue of energy channelling into high-frequency motions that attenuate in short distances from the pile. The presented contour patterns do not resemble the wavefield at any time instant

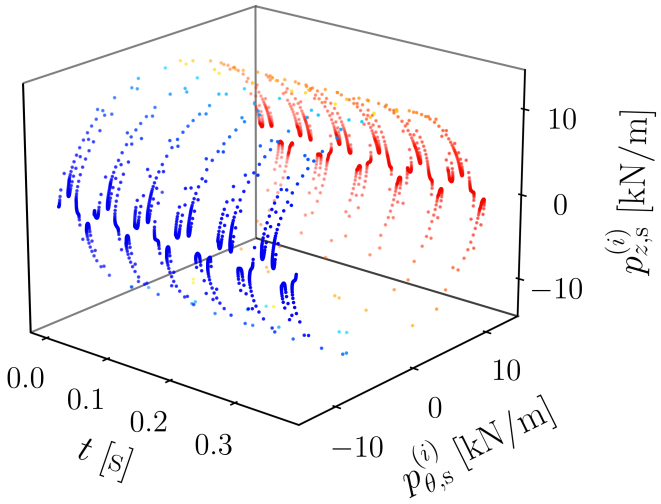

Figure 7: Friction force trajectory at $z_i = 3.0$ m and $u_\mathrm{R} = 5.5$ m; the color of the markers is based on the ratio of circumferential to total friction force, i.e. ranging from -1 (blue) to 1 (red).

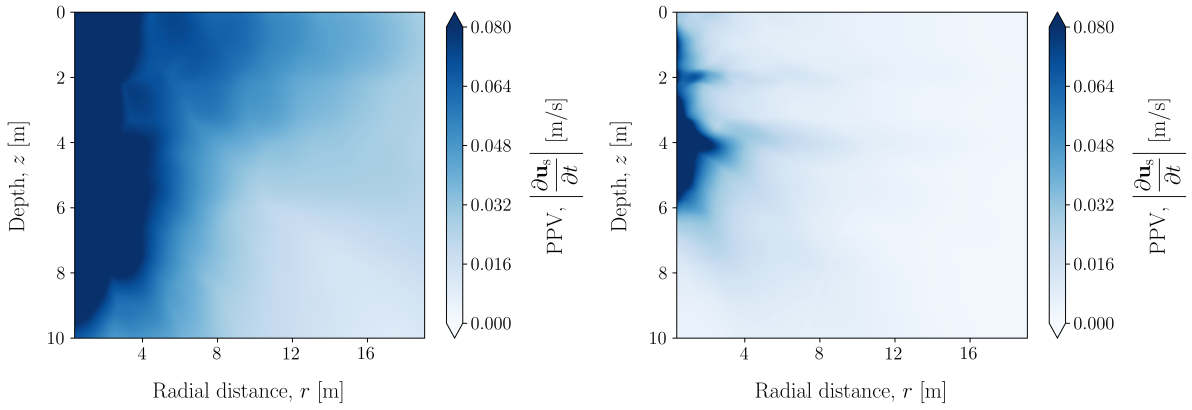

(a) VH_1 (b) GDP_1

Figure 8: PPVs (surface and interior soil domain) for VH_1 and GDP_1 at pile penetration $u_\mathrm{R} = 5.5$ m.

(i.e. response snapshot), but correspond to the collection of the PPVs for all soil material points attained during a time window sufficient for stationary response. To better comprehend the resulting soil response, Fig. 9 presents the wave field for the two driving cases, where the contour color corresponds to the vertical displacement and the mesh points are deformed based on the in-plane motion ($u_{r,\mathrm{s}}$, $u_{z,\mathrm{s}}$) for a certain time instant. As can be seen, the displacement amplitudes of GDP are largely reduced compared to vibro-driving, aligned with the previous results. It is remarked that the wave motion vanishes for both cases below 10.5 m, testifying the superb capabilities of PMLs as absorbing boundary layers.

To investigate further the characteristics of the induced soil motion, the soil particle trajectories ($u_{r,\mathrm{s}}$, $u_{z,\mathrm{s}}$) at the ground surface are presented in Fig. 10 for different radial distances (SV-P wavefield). In the pile vicinity, these trajectories are vertically polarized and as the radius

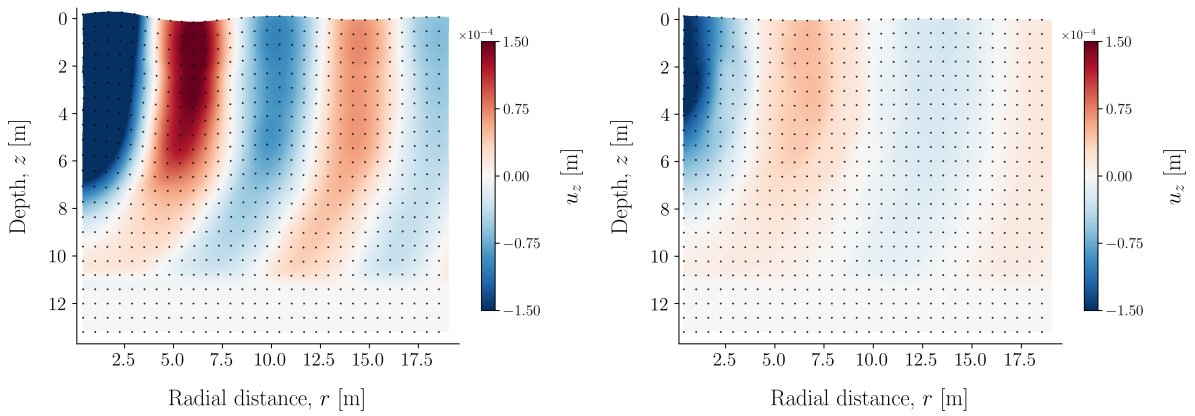

(a) VH_1 (b) GDP_1

Figure 9: Displacement field for VH_1 and GDP_1 at pile penetration $u_R = 3.5$ m; the contour color corresponds to $u_{z,s}$, whereas the deformed mesh considers both $u_{z,s}$ and $u_{r,s}$.

increases retrograde elliptical orbits are formed (typical of Rayleigh waves) in both cases [14]. However, the magnitude of the soil particle trajectories during vibro-driving is appreciably larger than the one resulting from GDP. In Fig. 10b, an additional discrepancy can be observed in the respective orbit patterns, i.e. the soil motion showcases richer frequency content in the case of GDP. Energy redistribution and coupling of the interacting super-harmonics of vertical and circumferential friction components lead to this outcome. Finally, comparison of the two orbit sets reveals a higher rate of orbit size reduction in GDP, associated with the preceding mechanisms.

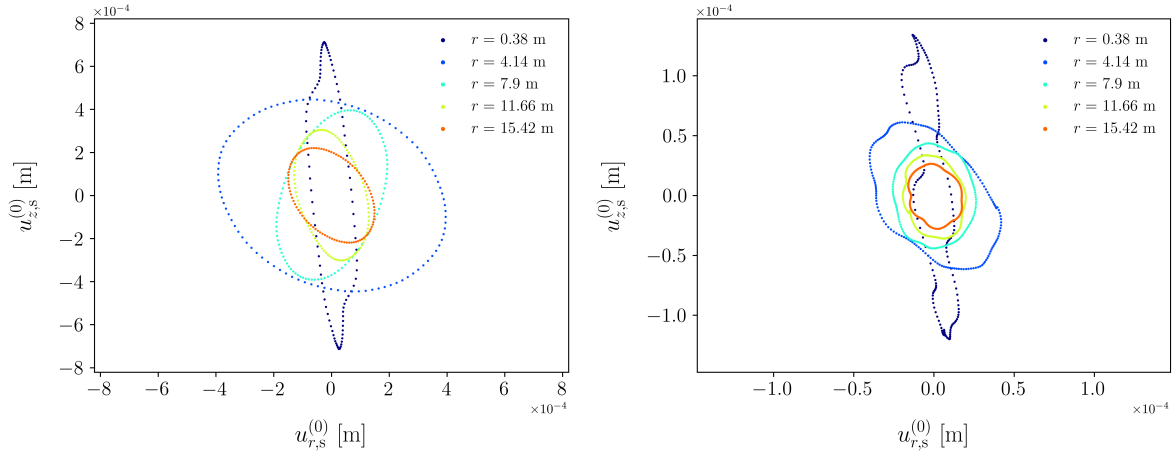

(a) VH_1 (b) GDP_1

Figure 10: Trajectories of soil particle motion $(u_{r,s}^{(0)}, u_{z,s}^{(0)})$ at the ground surface for VH_1 and GDP_1 at pile penetration $u_R = 5.5$ m.

4. Conclusions

This paper focuses on a new (mono)pile installation technology, namely the Gentle Driving of Piles. The installation process is studied by means of a numerical modelling framework -

applicable to both axial vibratory and GDP methods - with a view to investigate the driving mechanisms of GDP. A brief outline of GDP and the associated field campaign is provided, with key features being the successful proof of concept and the promising installation performance of GDP. The presented numerical model is utilized to study the previous installation tests; comparison of model predictions with field data is favourable and numerical analyses elucidate the mechanics of GDP. The friction forces are continuously diverted due to the high-frequency torsion and this redirection manifests as the main driving mechanism of GDP. Finally, a numerical comparison of GDP and axial vibro-driving showcases that the soil disturbance induced by GDP is significantly lower in magnitude and accompanied by greatly abated Rayleigh waves, energy transfer in higher frequencies and disturbance localization in the pile vicinity.

Acknowledgments
This research is associated with the GDP project in the framework of the GROW joint research program. Funding from "Topsector Energiesubsidie van het Ministerie van Econsomische Zaken" under grant number TE-HE117100 and financial/technical support from the following partners is gratefully acknowledged: Royal Boskalis Westminster N.V., CAPE Holland B.V., Deltares, Delft Offshore Turbine B.V., Delft University of Technology, ECN, Eneco Wind B.V., IHC IQIP B.V., RWE Offshore Wind Netherlands B.V., SHL Offshore Contractors B.V., Shell Global Solutions International B.V., Sif Netherlands B.V., TNO, and Van Oord Offshore Wind Projects B.V.

References

[1] Ramírez L, Fraile D and Brindley G 2021 *WindEurope*
[2] Merchant N D 2019 *Environmental Science & Policy* **92** 116–123
[3] Tsouvalas A 2020 *Energies* **13** 3037
[4] Rodger A and Littlejohn G 1980 *Géotechnique* **30** 269–293
[5] Metrikine A V, Tsouvalas A, Segeren M L A, Elkadi A S K, Tehrani F S, Gómez S S, Atkinson R, Pisanò F, Kementzetzidis E, Tsetas A, Molenkamp T, van Beek K and de Vries P 2020 Gdp: A new technology for gentle driving of (mono)piles *Proceedings of the 4th International Symposium on Frontiers in Offshore Geotechnics, Austin, TX, USA, 16–19 August 2020*
[6] Tsetas A, Tsouvalas A, Gómez S, Pisanò F, Kementzetzidis E, Molenkamp T, Elkadi A and Metrikine A 2023 *Ocean Engineering* **270** 113453
[7] Kementzetzidis E, Pisanò F, Tsetas A and Metrikine A 2023 *Journal of Geoenvironmental and Geotechnical Engineering*
[8] Tsetas A, Tsouvalas A and Metrikine A V 2023 *International Journal of Solids and Structures* **269** 112202
[9] Timoshenko S P and Woinowsky-Krieger S 1959 *Theory of plates and shells* (McGraw-hill)
[10] Kausel E and Roësset J M 1981 *Bulletin of the seismological Society of America* **71** 1743–1761
[11] de Oliveira Barbosa J M, Park J and Kausel E 2012 *Computer Methods in Applied Mechanics and Engineering* **217** 262–274
[12] Kausel E and Peek R 1982 *Bulletin of the Seismological Society of America* **72** 1459–1481
[13] Krack M and Gross J 2019 *Harmonic balance for nonlinear vibration problems* vol 1 (Springer)
[14] Masoumi H, Degrande G and Lombaert G 2007 *Soil Dynamics and Earthquake Engineering* **27** 126–143